Optomechanical Collective Effects in Surface-Enhanced Raman Scattering from Many Molecules

Yuan Zhang,* Javier Aizpurua,* and Ruben Esteban*

Cite This: https://dx.doi.org/10.1021/acsphotonics.0c00032 **Read Online**

ACCESS | Metrics & More | Article Recommendations | Supporting Information

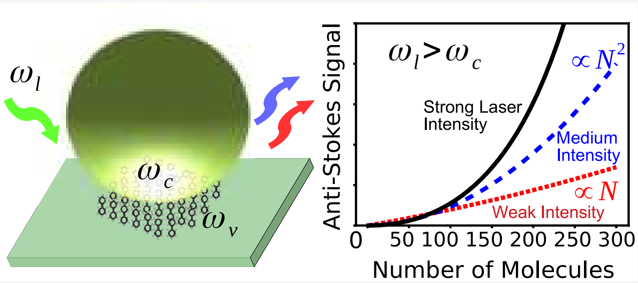

ABSTRACT: The interaction between molecules is commonly ignored in surface-enhanced Raman scattering (SERS). Under this assumption, the total SERS signal is described as the sum of the individual contributions of each molecule treated independently. We adopt here an optomechanical description of SERS within a cavity quantum electrodynamics framework to study how collective effects emerge from the quantum correlations of distinct molecules. We derive analytical expressions for identical molecules and implement numerical simulations to analyze two types of collective phenomena: (i) a decrease of the laser intensity threshold to observe strong nonlinearities as the number of molecules increases, within very intense illumination, and (ii) identification of superradiance in the SERS signal, namely a quadratic scaling with the number of molecules. The laser intensity required to observe the latter in the anti-Stokes scattering is relatively moderate, which makes it particularly accessible to experiments. We treat the system on the basis of the individual molecules and demonstrate that for ideal systems with identical molecules this approach is equivalent to a description based on collective modes. The basis of individual molecules also allows for describing in a straightforward manner more general systems where the molecules might have different vibrational properties or suffer from pure-dephasing processes. Our results show that the collective phenomena can survive in the presence of the homogeneous and inhomogeneous broadening that might influence experimental results.

KEYWORDS: *surface-enhanced Raman scattering, collective effects, cavity optomechanics, superradiance, surface plasmons*

The interaction between molecular vibrations and photons of an external laser as measured in surface-enhanced Raman scattering (SERS)[1,2] spectroscopy is strongly enhanced by the presence of nearby metallic nanostructures acting as effective optical nanoantennas,[3,4] such as nanorods,[5−8] nanostars,[9−11] nanoparticle dimers,[12−16] nanoparticle-on-a-mirror configurations,[17,18] and atomic force microscope or scanning tunnelling microscope (STM) tips.[19−26] This enhancement is partially attributed to the chemical interaction between the molecules and the metal,[27] but it is mainly boosted by the strong increase of the electromagnetic field strength near the nanostructures[1] due to the collective excitation of electrons in the metal, i.e. localized surface plasmon polaritons. Because the characteristic narrow Raman peaks can be associated with unique vibrational frequencies of molecules, SERS is standardly applied to detect particular molecular fingerprints and to characterize and track minute amounts of analytes[28−31] (including single molecules[32−34]) for biology and medicine.[35]

Most SERS measurements have been successfully interpreted within classical or semiclassical theories,[1,38] but recent experiments using well-controlled metallic nanostructures and precise positioning of molecules[12,17,19] might allow us to reach conditions where the quantum nature of the molecular vibration-plasmon interaction becomes relevant. In the past few years, a cavity quantum electrodynamics (QED) description of SERS has been developed[39−42] by using second-quantization to model both photonic and vibrational excitations. This description is formally analogous to the one typically used in cavity optomechanics,[43] but with orders-of-magnitude larger losses and coupling strength. This molecular optomechanical approach is able to predict not only the population of the molecular vibrations and the Stokes and anti-Stokes SERS signal in standard situations but also many other intriguing effects, such as Raman-induced plasmon resonance shifts, higher-order Stokes scattering, complex Raman photon correlations, heat-transfer between molecules, and a strongly nonlinear scaling of the Stokes and anti-Stokes signal with laser intensity that can even lead to a divergence on the emitted signal (known as parametric instability in cavity optomechanics).[39,40,42,44,45]

While previous works focused mostly on single molecules, we provide here a thorough study of SERS when many molecules are present. Qualitatively different behaviors arise when this

Received: January 8, 2020
Published: April 6, 2020

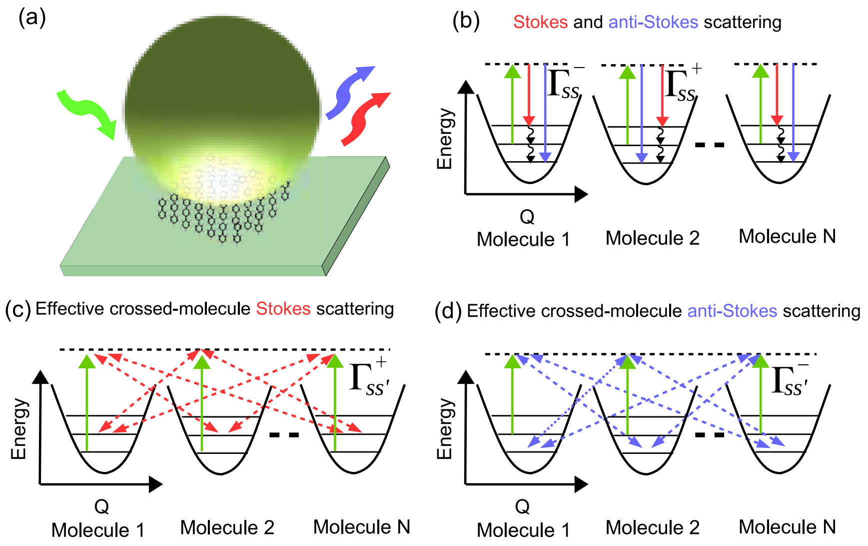

Figure 1. (a) Schematics of the SERS system. An ensemble of molecules is located in a gap between a gold nanostructure and a gold substrate. The molecules interact with the plasmonic system, which is excited by an external laser (green arrow), and the emission rate of Stokes (red arrow) and anti-Stokes (blue arrow) Raman photons is enhanced by the plasmonic response of the metallic nanostructure. (b) Diagram of the Raman process when the (plasmon-mediated) interactions between different molecules are assumed to be absent. The vibrational mode of each molecule is modeled as a harmonic oscillator with equally spaced energy levels in a parabolic potential energy surface (with respect to the normal mode coordinate Q). The plasmon-enhanced Stokes (vertical red lines) and anti-Stokes (vertical blue lines) scattering occur via virtual levels (horizontal dashed lines), excited by the plasmon-enhanced local field (green vertical lines). Phonon decay of individual molecules are also included (vertical wavy arrows). (c, d) Schematic representation of collective effects in the (c) Stokes and (d) anti-Stokes Raman scattering from several molecules. Plasmon-mediated interactions between the molecules establishing molecule−molecule correlations are represented with red dashed double arrows (Stokes, c) and blue dashed double arrows (anti-Stokes, d). The parameters $\Gamma_{ss}^{\pm}$ and $\Gamma_{ss'}^{\pm}$ ($s \neq s'$) characterizing the processes in (b, c, d) are described in the text.

situation is studied by the optomechanical description and by the standard classical treatment. The latter typically assumes that the molecules can be considered as independent, i.e. without interaction among them, so that the signal from N identical molecules simply corresponds to N times the signal from a single molecule. On the other hand, the optomechanical description suggests that the molecules can interact with each other via their coupling to the plasmonic structure, leading to collective effects under adequate conditions. For example, it has been pointed out theoretically[39] that the presence of many molecules can facilitate reaching the parametric instability at lower laser intensity. The collective response has also been invoked in the design of a photon up-conversion device based on SERS[46] and to explain a recent experiment[47] that reveals a nonlinear dependence of the Stokes SERS signal on the pulsed laser intensity. These works consider the presence of a collective bright mode that couples with the plasmon with a coupling strength that scales with the square root of the number of molecules. In other related contexts, collective interactions have been studied in Raman experiments with exquisitely controlled atoms at ultralow temperatures and are now applied routinely to study a variety of interesting phenomena, such as superradiant Raman lasing,[48] spin-squeezing,[49] and quantum phase transitions.[50] In these systems the Raman signal can scale quadratically with the number of atoms.[51]

In short, the optomechanical description suggests that novel collective effects can emerge in experiments, but most SERS measurements are regularly interpreted without considering these effects. Motivated by this appealing opportunity, we study in this paper under which conditions the collective effects can emerge in realistic SERS experiments. With this objective in mind, we extend the molecular optomechanical description of nonresonant Raman to the case of many molecules (see sketch in Figure 1a), which naturally incorporates the quantum correlations between different molecules that are the origin of these collective effects. We first focus on a simple system that consists of identical molecules and derive analytic expressions to identify two kinds of collective effects: (i) a quadratic increase of the Stokes and, more significantly, the anti-Stokes signal with an increasing number of molecules N and (ii) a decrease of the laser intensity required to observe the parametric instability or a saturation of the vibrational population for an increasing N. The latter is connected with the cooling of mechanical oscillators that is often observed in other optomechanical systems.[43] We derive the relevant equations in the basis of individual molecules, which allows us to recover the results obtained from a collective-mode description for simple scenarios and also to incorporate in a natural way other effects such as the homogeneous broadening of the molecules caused by e.g. loss-induced dephasing or the inhomogeneous broadening due to slight variations in the vibrational frequency of different molecules. Our study shows that collective effects are robust to both types of broadening, a beneficial feature for experimental demonstrations. Last, we also show how the Raman lines can be shifted, narrowed, or broadened for very intense illumination and how the shifting of the plasmonic resonance due to the optomechanical interaction affects the response (we discuss these additional effects and their dependence on the number of molecules in the Supporting Information).

■ SYSTEM AND MODEL

We study the Raman scattering from an arbitrary number of molecules that interact with a plasmonic nanostructure, as sketched in Figure 1a. We consider biphenyl-4-thiol (BPT) molecules as canonical molecular species coupled to an optimized plasmonic system, such as a metallic nanoparticle on a mirror configuration[17] or a metallic STM tip over a metallic substrate.[19] Our model assumes that the molecules are sufficiently far apart so that they interact with each other only via their coupling with the plasmonic excitation of the nanostructure, and thus the model is more suitable for systems where the molecules are not closely packed.

We consider the vibrational mode of the BPT molecule[47] with energy $\hbar\omega_s = 196.5$ meV (frequency 1585 cm^{-1}) due to its large Raman tensor. We consider $R_s = 316.23\ \epsilon_0 Å^2 \mathrm{amu}^{-1/2}$ for the value of the Raman tensor component along the optimal direction. Here, ϵ_0 and amu are the vacuum permittivity and the atomic mass unit, respectively, and $\hbar$ is Planck's reduced constant. The value of R_s is due to not only the intrinsic properties of the molecule but also assumes a moderate chemical interaction with the metallic surfaces (chemical Raman enhancement). For simplicity, we neglect any possible infrared activity of the molecular vibrations, so that different molecules couple only with each other via Raman processes. The subindex s distinguishes between molecules, which is useful for molecules with different vibrational frequencies as considered later on. We consider nonresonant SERS and thus do not include the electronic excited states of the molecule explicitly. A cavity QED description of resonant SERS has also been developed and used to analyze the emission from single molecules.[52,53] In addition, we assume that the potential energy surface (of the electronic ground state) depends quadratically on the normal mode coordinates and thus the vibrations can be modeled as harmonic oscillators via the Hamiltonian $H_{vib} = \sum_s \hbar\omega_s b_s^\dagger b_s$, where $b_s^\dagger$ and b_s are the bosonic creation and annihilation operators of the vibrational excitations of the different molecules, respectively.[2,40] The incoherent coupling of the molecular vibrations with the environment results in a phonon decay rate that we assume to be small $\hbar\gamma_s = 0.07$ meV[45,47] (except when otherwise stated), a thermal phonon population $n_s^{th} = [e^{\hbar\omega_s/k_B T} - 1]^{-1} \approx 4 \times 10^{-4}$ at temperature $T = 290K$ (k_B is the Boltzmann constant), and a vibrational pure-dephasing rate (homogeneous broadening) χ_s.[54] We set χ_s initially to zero and analyze its influence on the system later on. The incoherent processes are included in our description via Lindblad terms in the quantum master equation (see below).

We assume that the metallic nanostructure is surrounded by vacuum and that its plasmonic response is dominated by a single Lorentzian-like cavity mode,[55,56] characterized by an energy $\hbar\omega_c = 1.722$ eV (wavelength 720 nm), a damping rate $\hbar\kappa = 200$ meV and an effective mode volume $V_{eff} = 327$ nm^3. This volume is significantly below the diffraction limit but is large enough to accommodate many molecules and is well within values achievable with plasmonic structures.[57,58] We model this cavity mode within the canonical quantization scheme[40] as a harmonic oscillator characterized by the Hamiltonian $H_{cav} = \hbar\omega_c a^\dagger a$, where $a^\dagger$ and a are bosonic creation and annihilation operator of the plasmonic excitation, respectively. This model can be extended in a straightforward manner to a system with an arbitrary plasmonic response.[55,59] In addition, the plasmonic cavity is excited by a laser of angular frequency ω_l as described by the Hamiltonian $H_{las} = i\hbar\Omega(a^\dagger e^{-i\omega_l t} - a e^{i\omega_l t})$ in the rotating wave approximation (RWA). $\Omega = \frac{\kappa}{2}\sqrt{\frac{\epsilon_0 V_{eff}}{2\hbar\omega_c}} K \sqrt{\frac{2 I_{las}}{\epsilon_0 c}}$ is the strength of the coupling between the plasmonic resonance and the excitation laser[40,56] with $K = 206$ the maximum enhancement of the electric field amplitude at resonance, I_{las} the laser intensity, and c the speed of light in vacuum.[47]

The molecular vibrations interact with the plasmonic mode via the molecular optomechanical coupling[39−41] $H_{int} = -a^\dagger a \sum_s \hbar g_s (b_s^\dagger + b_s)$. The (real valued) optomechanical coupling strength $g_s = f_s \sqrt{\frac{\hbar}{8\omega_s}} \frac{R_s \omega_c}{\varepsilon_0 V_{eff}}$ depends on the properties of the molecular vibrations, such as the Raman tensor, and those of the plasmon, such as the effective mode volume V_{eff}.[39−41] The factor $f_s \leq 1$ accounts for the position and orientation of the molecule and is one in the optimal case. In our system, we obtain $\hbar g_s = 0.086$ meV (with $f_s = 1$) as a representative value, which is much stronger than the typical values in standard cavity optomechanical systems but is still relatively moderate in the context of molecular optomechanics.[41]

We model the dynamics of this lossy system with the standard quantum master equation[60] for the reduced density operator ρ with the full Hamiltonian $H = H_{vib} + H_{cav} + H_{las} + H_{int}$ describing the coherent dynamics, and the Lindblad superoperators incorporating incoherent processes, such as plasmon damping, phonon decay, thermal pumping and dephasing of molecular vibrations. Further on, we can simplify the solution of the master equation dramatically by adiabatically eliminating the plasmonic degree of freedom after linearizing the Hamiltonian H_{int}. As a result, we obtain an effective master equation for the reduced density operator ρ_v of the molecular vibrations, which describes the dynamics associated with the vibrational (incoherent) noise operator $\delta b_s = b_s - \beta_s$, where $\beta_s = \mathrm{tr}\{b_s \rho\}$ is the coherent amplitude. From the effective master equation we obtain the equations for the incoherent phonon population $n_s \equiv \langle \delta b_s^\dagger \delta b_s \rangle = \mathrm{tr}\{\delta b_s^\dagger \delta b_s \rho_v\}$ and the noise correlations $c_{ss'} \equiv \langle \delta b_s^\dagger \delta b_{s'} \rangle$ ($s \neq s'$) as well as for the noise amplitudes $\langle \delta b_s \rangle$ (or $\langle \delta b_s^\dagger \rangle$). We show in section S5.1 of the Supporting Information that the incoherent phonon population dominates over the coherent value $|\beta_s|^2$ except for extremely intense lasers. The Raman spectra can be obtained by applying the quantum regression theorem[61] to the equations for the $\langle \delta b_s \rangle$ and $\langle \delta b_s^\dagger \rangle$. Significantly, we find that the Stokes and anti-Stokes scattering are affected not only by the dynamics of individual molecules but also by the molecule−molecule correlations. More details on the derivation, the exact equations, and the involved approximations are provided in the Methods section and in sections S1 and S2 of the Supporting Information.

In our model the plasmonic mode acts as a structured reservoir and affects the vibrational dynamics by introducing: (i) a shift of the vibrational frequencies, in a similar way as the Lamb shift;[62,63] (ii) plasmon-mediated coherent coupling between each pair of molecules; (iii) incoherent pumping of each vibration at rate Γ_{ss}^+; (iv) incoherent damping at rate Γ_{ss}^-; and (v) plasmon-mediated incoherent coupling of the vibrations at rate $\Gamma_{ss'}^+, \Gamma_{ss'}^-$ ($s \neq s'$). The last four sets of parameters (corresponding to iii−v) are particularly important for the phenomena discussed in this work. Here, the superscripts "+" and "−" indicate that the parameters are evaluated from the spectral density of the plasmon at the Stokes $\omega_l - \omega_s$ (+) and anti-Stokes $\omega_l + \omega_s$ (−) frequencies. The exact expressions of these parameters are given in section S1.2 of the Supporting Information, but we note that all of them are proportional to the laser intensity. As an example, for two molecules with the same vibrational frequency $\omega_s = \omega_{s'}$ but different optomechanical coupling to the plasmonic cavity $g_s \neq g_{s'}$, the rates $\Gamma_{ss'}^+$ and $\Gamma_{ss'}^-$ follow expressions similar to those of single molecules[40,41] as

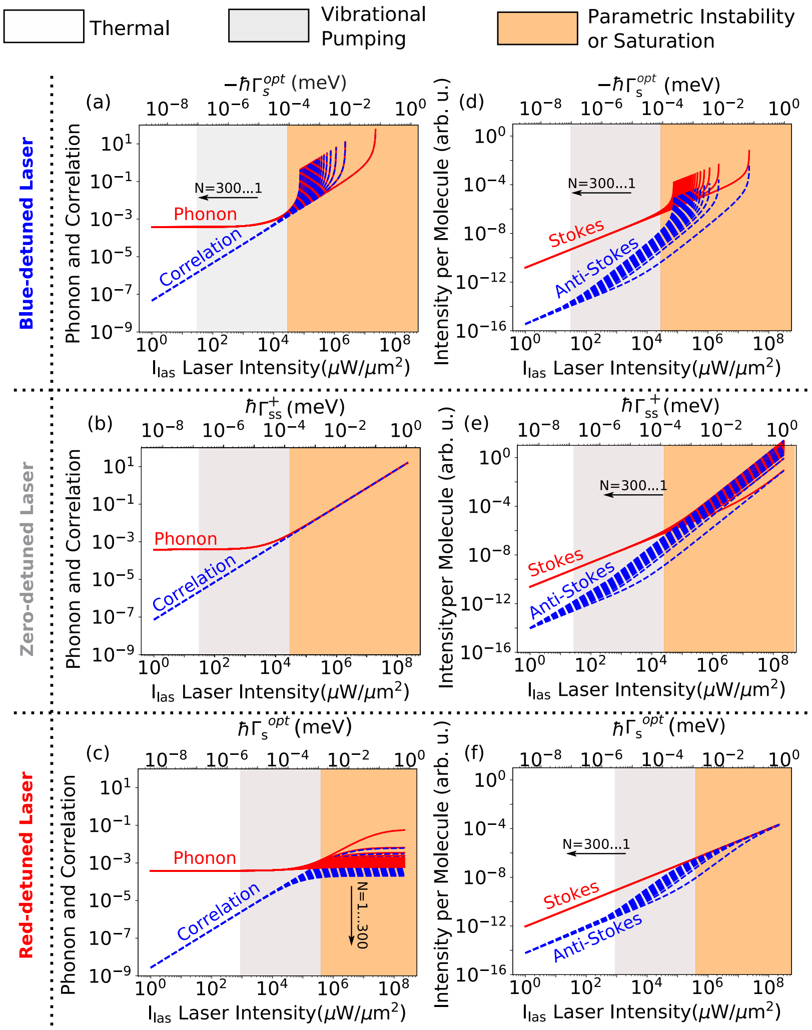

Figure 2. Influence of the number of identical molecules N (increases as 1, 10, 20, ..., 300) on (a, b, c) the incoherent phonon population n_s (red solid lines) and the noise correlation $c_{ss'}$ (blue dashed lines) and on (d, e, f) the frequency-integrated intensity of the Stokes (red solid lines) and anti-Stokes (blue dashed lines) scattering *per molecule* for increasing laser intensity I_{las}. For reference we indicate in the upper axis the values of $\hbar\Gamma_s^{opt}$ or $\hbar\Gamma_{ss}^{+}$ for each I_{las}. Notice that the noise correlations are not defined for $N = 1$. We consider systems illuminated with a laser (a,d) blue-, (b,e) zero-, and (c,f) red-detuned with respect to the shifted plasmon resonance ($\hbar\Delta\omega = \hbar(\omega_l - \omega_c')$ =236 meV, 0, −236 meV), respectively. The white and gray shaded area indicate the thermal and vibrational pumping regime, respectively, and the orange shaded area signals the regime of very intense laser illumination showing (a, d) parametric instability or (c, f) saturation of the phonon population. We consider phonon decay rate $\hbar\gamma_s = 0.07$ meV, temperature $T = 290$ K and no homogeneous broadening $2\chi_s = 0$. For other parameters see the text.

$$\Gamma^{\pm}_{ss'} \propto \frac{I_{las} g_s g_{s'}}{(\omega_c' - \omega_l)^2 + (\kappa/2)^2} \frac{\kappa}{(\omega_c' - \omega_l \pm \omega_s)^2 + (\kappa/2)^2} \qquad (1)$$

with $\omega_c' = \omega_c - 2\sum_s g_s \mathrm{Re}\beta_s$ the plasmonic cavity frequency accounting for the slight shift $2\sum_s g_s \mathrm{Re}\beta_s$ induced by the vibrations (analogue to the Lamb shift). The advantage of this approach is that it results in a closed set of equations solvable for many molecules (see section S2 in the Supporting Information).

To conclude, Figure 1b−d sketches an intuitive picture of the parameters $\Gamma^{+}_{ss'}$,$\Gamma^{-}_{ss'}$. More precisely, Γ^{+}_{ss} (Γ^{-}_{ss}) corresponds to the transition rates from lower (higher) to higher (lower) vibrational states of *individual molecules* that are already present in the absence of any collective effect, as represented by the red (blue) arrows in Figure 1b and discussed in previous works on single-molecule optomechanical SERS.[40,41] On the other hand, $\Gamma^{+}_{ss'}$ and $\Gamma^{-}_{ss'}$ (with $s \neq s'$) emerge from the full collective situation, describe the plasmon-mediated interaction between molecule s and s', and introduce additional interaction paths to excite or de-excite vibrational states, as schematically represented by the red arrows in Figure 1c and the blue arrows in Figure 1d, respectively.

COLLECTIVE EFFECTS IN RAMAN SCATTERING OF IDENTICAL MOLECULES

In this section, we focus on the simplest case of N identical molecules and no homogeneous broadening, to identify under which conditions collective effects can emerge. Throughout the paper, the term *identical molecules* implies not only that the intrinsic properties of the molecular vibrations are the same but also that they couple to the plasmon with the same strength. We show in Figure 2 the incoherent phonon population and the noise correlation (a, b, c), and the (frequency-integrated) Stokes and anti-Stokes intensity (d, e, f) for different number of molecules N ($N = 1, 10, 20, ..., 300$) in the cavity, as a function of laser intensity I_{las} (from 1 μW/μm^2 to 10^8 μW/μm^2, corresponding to $\hbar\Omega$ from 1.295 meV to 12.95×10^3 meV). The Raman signal in (d, e, f) is normalized by N, i.e. the scattering per molecule, so that the collective effects are manifested by a change of this quantity with increasing N. We also consider different frequency detunings, $\Delta\omega = \omega_l - \omega_c'$, between the laser excitation and the plasmonic resonance to show that, consistent with the work on single molecules,[40] different trends are observed when the strong laser illumination is blue-detuned ($\hbar\Delta\omega = 236$ meV > 0, Figure 2a, d), zero-detuned ($\Delta\omega = 0$, Figure 2b, e) and red-detuned ($\hbar\Delta\omega = -236$ meV < 0, Figure 2c, f). To simplify the discussion, in all the calculations we fix the detuning $\omega_l - \omega_c'$ with respect to the shifted plasmon resonance ω_c' by slightly shifting ω_l as the laser intensity is increased (see section S5.5 in the Supporting Information for results with ω_l fixed).

To understand the results in Figure 2, we derive analytical expressions by taking advantage of the permutation symmetry of identical molecules (see section S3 in the Supporting Information). We find that the intensity integrated over the Stokes and anti-Stokes lines can be expressed as

$$I^{st} \propto (\omega_l - \omega_s)^4 \Gamma_{ss}^{+}[N(1 + n_s) + N(N - 1)c_{ss'}] \tag{2}$$

$$I^{as} \propto (\omega_l + \omega_s)^4 \Gamma_{ss}^{-}[N n_s + N(N - 1)c_{ss'}] \tag{3}$$

where the factor N and $N(N-1)$ originate from the sum over all identical molecules and all identical molecular pairs, respectively. The latter leads to the emergence of the collective effects when the noise correlations $c_{ss'}$ are sufficiently large. The factor $(\omega_l \mp \omega_s)^4$ originates from the frequency-dependence of dipolar emission and, for simplicity, is ignored in our calculations.

Further, the noise correlation $c_{ss'}$ and the incoherent phonon population n_s are given by

$$c_{ss'} = \frac{\Gamma_{ss}^{+} - \Gamma_s^{opt} n_s^{th}}{\gamma_s + N\Gamma_s^{opt}} \tag{4}$$

$$n_s = n_s^{th} + \frac{\Gamma_{ss}^{+} - \Gamma_s^{opt} n_s^{th}}{\gamma_s + N\Gamma_s^{opt}} = n_s^{th} + c_{ss'} \tag{5}$$

where eq 4 is defined for $N > 1$ and we have defined the optomechanical damping rate $\Gamma_s^{opt} = \Gamma_{ss}^{-} - \Gamma_{ss}^{+}$ of a single molecule[40,43,47] (with $\Gamma_{ss}^{\pm} \propto I_{las}$, see eq 1). The denominator, $\gamma_s + N\Gamma_s^{opt}$, in these expressions can be understood as a modification of the effective phonon decay rate due to the optomechanical damping rate. We observe that the incoherent phonon population n_s is equal to the noise correlation $c_{ss'}$ plus the thermal population n_s^{th}. The noise correlation is built through the plasmon-mediated molecule−molecule interaction (notice $\Gamma_{ss'}^{\pm} = \Gamma_{ss}^{\pm}$ for identical molecules). In addition, we note that eqs 2−5 can also be derived within a collective oscillator model, as detailed in section S4 of the Supporting Information. The collective oscillator model is particularly well suited for the simple situation of N identical molecules and no homogeneous broadening, resulting in a simple picture in terms of a bright collective vibrational mode[39,64] that couples with the plasmonic mode with an effective coupling strength proportional to $\sqrt{N}$. On the other hand, the basis of individual molecules that we employ can be applied in a straightforward manner to more general situations.This basis also reveals in a transparent manner the important role of the noise correlations to establish collective effects.

Inserting eqs 4 and 5 into eqs 2 and 3, we obtain the compact expressions for the Raman signal

$$I^{st} \propto (\omega_l - \omega_s)^4 \Gamma_{ss}^{+}\left(N(1 + n_s^{th}) + N^2 \frac{\Gamma_{ss}^{+} - \Gamma_s^{opt} n_s^{th}}{\gamma_s + N\Gamma_s^{opt}}\right) \tag{6}$$

$$I^{as} \propto (\omega_l + \omega_s)^4 \Gamma_{ss}^{-}\left(N n_s^{th} + N^2 \frac{\Gamma_{ss}^{+} - \Gamma_s^{opt} n_s^{th}}{\gamma_s + N\Gamma_s^{opt}}\right) \tag{7}$$

Equations 1−7 allow for understanding the collective effects revealed by Figure 2. To this end, it is useful to distinguish three regimes as identified previously for single molecules[40] (coded with different background colors in Figure 2) for different laser intensities.

Weak and Moderate Laser Illumination: Thermal and Vibrational Pumping Regimes. For weak and moderate laser intensity I_{las}, the vibrational damping and pumping rates given by eq 1 for $s = s'$ (and thus the optomechanical damping rate) are small enough so that they do not affect the effective phonon decay rate for any N, i.e. $\gamma_s + N\Gamma_s^{opt} \approx \gamma_s$, and thus $c_{ss'} \approx \Gamma_{ss}^{+}/\gamma_s \propto I_{las}$ (for $n_s^{th} \ll 1$). As a consequence, the phonon population (eq 5) adopts a very simple form, $n_s \approx n_s^{th} + \Gamma_{ss}^{+}/\gamma_s$, with a constant thermal population n_s^{th} and a term $\Gamma_{ss}^{+}/\gamma_s \propto I_{las}$ proportional to the laser intensity that accounts for the creation of phonon by Stokes scattering, also known as vibrational pumping.[36−38] The noise correlations (eq 4) follow the same linear dependence with I_{las}, but do not depend on the thermal population, i.e. $c_{ss'} \approx \Gamma_{ss}^{+}/\gamma_s \propto I_{las}$.

We can now identify the first two regimes. When the laser intensity I_{las} is small enough, the thermal contribution dominates the incoherent phonon population, $n_s \approx n_s^{th}$, and we are thus in the so-called thermal regime (white-shaded area in Figure 2). On the other hand, for moderate I_{las} the incoherent phonon population is largely induced by the vibrational pumping rate Γ_{ss}^{+} ($n_s \approx n_s^{th} + \Gamma_{ss}^{+}/\gamma_s$), and the system is in the vibrational pumping regime (gray shaded area in Figure 2).[38,40] The noise correlations follow the same expression ($c_{ss'} \approx \Gamma_{ss}^{+}/\gamma_s \propto I_{las}$) for both weak and moderate laser intensities but become significantly larger in the vibrational pumping regime. Notably, these expressions and the results in Figure 2a−c demonstrate that neither the incoherent phonon number nor the noise correlation depends on the number of molecules, and thus they do not manifest any collective effect, neither in the thermal nor in the vibrational pumping regime. Furthermore, all the trends discussed here are independent of the laser detuning.

We can now use the above analysis of the noise correlation and the incoherent phonon population to explain the evolution of the Raman signal in Figure 2d−f for weak and moderate I_{las}. The number of molecules can affect the Raman signal via its influence on the incoherent phonon population, or via the noise correlation that characterizes the molecule−molecule interaction (term scaling as N^2 in eqs 2 and 3). We focus first on the thermal regime, where both effects are negligible; that is, on the one hand $n_s \approx n_s^{th}$ and on the other hand $c_{ss'}$ remains too weak to significantly affect the emitted signal. As a consequence, the integrated Stokes (red lines) and anti-Stokes (blue lines) intensities normalized by N in Figure 2 are independent of the number of molecules and they scale linearly with laser intensity, as observed directly from eqs 2 and 3 (or eqs 6 and 7), which become $I^{st}/N \propto \Gamma_{ss}^{+}(1 + n_s^{th})$ and $I^{as}/N \propto \Gamma_{ss}^{-} n_s^{th}$ (notice $\Gamma_{ss}^{+} \propto I_{las}$ and $\Gamma_{ss}^{-} \propto I_{las}$). Thus, in the thermal regime the Raman scattering does not show the signature of collective effects.

On the other hand, in the vibrational pumping regime it is not possible to neglect the effect of the correlations $c_{ss'}$ on the Raman scattering or the linear dependence of the incoherent phonon population n_s on the laser intensity I_{las}. As identified previously for single molecules,[40,45] the linear dependence of n_s leads to a quadratic dependence of the anti-Stokes scattering on I_{las}. Further, eq 3 also indicates that as $c_{ss'}$ becomes larger the integrated anti-Stokes intensity acquires a contribution that scales quadratically with the number of molecules $I^{as} \propto N^2$ (see eq 7). The anti-Stokes intensity *per molecule* I^{as}/N thus becomes dependent on the number of molecules for all laser detunings, as clearly revealed by the blue lines in Figure 2d−f, which is the signature of the first collective effect. The N^2 scaling of the scattering corresponds to a superradiant behavior, similar to the superradiant Raman scattering of cold atoms[51,65] or the single-photon superradiance from molecular or atomic electronic transitions.[66,67] This superradiant SERS emission can be understood as the result of the constructive interference of the coherent anti-Stokes scattering from the different strongly correlated molecules. As the intensity increases and the vibrational pumping becomes the preferential excitation mechanism of the bright collective mode instead of thermal processes (section S4 in the Supporting Information), the molecular vibrations become strongly correlated (large $c_{ss'}$) and the anti-Stokes emission of the dipoles induced at the individual molecules interferes constructively, leading to the N^2 scaling. Equivalently, we can attribute this effect to the N^2 interaction paths of the anti-Stokes scattering shown in Figure 1d that become relevant for sufficiently large noise correlations between different molecules.

It is also worthwhile to note that the term proportional to N^2 in eq 3 also scales with I_{las}^2 (for $c_{ss'} \propto I_{las}$). Thus, the quadratic dependence of the anti-Stokes signal with the laser intensity I_{las} becomes easier to be observed in Figure 2d−f as N is increased. Last, the Stokes intensity also acquires a contribution scaling as $N^2 I_{las}^2$ (eq 2). The absolute strength of this superradiant scattering is similar to the one found for the anti-Stokes signal. However, this quadratic term adds to the linear contribution that dominates the scattering in the thermal regime (the terms proportional to N in eqs 2 and 3), which is significantly larger for the Stokes than for the anti-Stokes signal (because of $n_s^{th} \ll 1$). Thus, it is harder to appreciate this quadratic contribution in the Stokes signal in Figure 2d−f. We also note that, as the ratio of the anti-Stokes and Stokes emission becomes dependent on the laser intensity and number of molecules, it can be challenging to extract the local temperature from this ratio.[29,39]

We can quantify the different behavior of the Stokes and anti-Stokes signals more rigorously by estimating quantitatively the laser intensity above which the collective (or superradiant) N^2 scaling becomes relevant. The terms scaling with $N^2 I_{las}^2$ in eqs 2 and 3 become relevant when the conditions $N\Gamma_{ss}^{+}/\gamma_s = 1$ and $N\Gamma_{ss}^{+}/\gamma_s = n_s^{th}$ are fulfilled for the Stokes and anti-Stokes intensity, respectively. In the derivation of these conditions, we have used the simplified expressions $c_{ss'} \approx \Gamma_{ss}^{+}/\gamma_s$ and $n_s \approx n_s^{th} + \Gamma_{ss}^{+}/\gamma_s$. Because of $n_s^{th} \approx 4 \times 10^{-4}$ the estimated threshold of the laser intensity is about 3 orders of magnitude smaller for the anti-Stokes scattering than for the Stokes scattering, as easily observed in Figure 2e. In our system, the quadratic scaling of the anti-Stokes signal appears at $I_{las} \approx 8 \times 10^3$ μW/μm^2 for a single molecule but could appear at only 27.5 μW/μm^2 for 300 molecules. The latter intensity is achievable with both continuous wave[45] and pulsed laser[47] and can be further reduced by working at low temperature (by reducing n_s^{th}), as shown in Figure S4 in the Supporting Information.

Strong Laser Illumination. In the following, we analyze the regime of strong laser illumination I_{las} (orange-shaded area in Figure 2). In contrast to previous regimes, there are very significant qualitative differences between the results obtained when the strong laser illumination is (a, d) blue-detuned, (b, e) zero-detuned, and (c, f) red-detuned with respect to the plasmonic resonance. As discussed for single molecules,[41] the key to understand these differences is that the optomechanical damping rate Γ_s^{opt} becomes sufficiently large compared to the intrinsic phonon decay γ_s, so that depending on the sign of Γ_s^{opt} the effective phonon decay rate $\gamma_s + N\Gamma_s^{opt}$ (i.e., the denominator in eqs 4 and 5) becomes larger or smaller than γ_s.

Blue-Detuned Laser Illumination: Parametric Instability. For blue-detuned illumination ($\hbar\omega_l = \hbar\omega_c' + 236$ meV), the pumping rate Γ_{ss}^{+} is larger than the damping rate Γ_{ss}^{-}, leading to a negative value of the optomechanical damping rate $\Gamma_s^{opt} < 0$ (see eq 1 and section S1.3 in the Supporting Information for the dependence of Γ_s^{opt} on laser frequency). As a result, the effective phonon decay rate $\gamma_s + N\Gamma_s^{opt} < \gamma_s$ reduces with increasing laser intensity I_{las} (notice $\Gamma_s^{opt} \propto -I_{las}$) and this leads to larger incoherent phonon population and noise correlation (see eqs 4 and 5). For sufficiently large I_{las}, the (negative) optomechanical damping rate becomes comparable to γ_s and the effective phonon decay rate approaches zero (i.e. the denominator in eqs 4 and 5 becomes vanishingly small). In this case, the incoherent phonon population n_s and the noise correlation $c_{ss'}$ become strongly nonlinear with I_{las} and finally diverge, as shown by the red and blue lines in Figure 2a, respectively. This divergence is known as parametric instability in cavity optomechanics,[43] and it is also seen in the Raman scattering[39,40] (blue and red lines in Figure 2d) because the Raman scattering depends on n_s and $c_{ss'}$ (eqs 2 and 3). In addition, we show in section S5.2 of the Supporting Information that, in this regime, the Raman lines become also narrower and shifted (an effect that depends on the number of molecules).

We can define the laser threshold intensity I_{thr} to achieve the parametric instability as the value for which the Raman scattering diverges ($\Gamma_s^{opt} = -\gamma_s/N$). Taking into account that $\Gamma_s^{opt} = \Gamma_{ss}^{-} - \Gamma_{ss}^{+} \propto -I_{thr}$ (eq 1), we obtain immediately that I_{thr} is reduced as the number of molecules increases, i.e. the second collective effect to be explored in detail here, which is clearly shown in Figure 2a, d. This collective effect can also be understood as the consequence of coupling the plasmonic mode with the collective bright mode of the molecules, with a coupling strength that scales[39] as $\sqrt{N}g_s$ (section S4 in the Supporting Information). I_{thr} is about 2.25×10^7 μW/μm^2 for a single molecule but reduces to 7.5×10^4 μW/μm^2 for 300 molecules. We note that such large intensities are difficult to reach in practice and can lead to effects not included here (for example, it may even dissociate the molecules[47]). Furthermore, for illumination larger than about 1.8×10^6 μW/μm^2 the coupling strength with the driving laser, Ω, becomes comparable to the plasmon frequency ω_c and the validity of the RWA approximation used in our model is compromised. In section S5.3 of the Supporting Information we examine how the collective effects are affected by the Raman tensor of the molecule. For instance, we show there how the threshold values for collective effects to emerge can be reduced if a larger R_s is considered (due for example to a larger chemical enhancement).

Zero-Detuned Laser Illumination: Superradiant Stokes Scattering. In Figure 2b, e, where the laser is resonant with the plasmonic mode ($\omega_l = \omega_c'$), the vibrational damping and pumping rate are equal, i.e. $\Gamma_{ss}^- = \Gamma_{ss}^+$, leading to a vanishing optomechanical damping rate $\Gamma_s^{opt} = 0$ (eq 1). The outcome of this situation is that the response maintains the same trends as in the vibrational pumping regime (where Γ_s^{opt} in the denominator of eqs 4 and 5 is negligible because of the small laser intensity I_{las}): the noise correlations and the incoherent phonon populations exhibit identical linear scaling with the laser intensity $c_{ss'} \approx n_s \approx \Gamma_{ss}^+/\gamma_s \propto I_{las}$ (Figure 2b and eqs 4 and 5), and the integrated Stokes and anti-Stokes signal increase quadratically with both the laser intensity and the number of molecules (Figure 2e and eqs 2 and 3 or eqs 6 and 7). It is indeed in the situation with zero-detuned laser illumination where the superradiant quadratic scaling of the Stokes scattering is easier to appreciate. We discuss in section S5.5 of the Supporting Information how extra features appear for very large laser intensities if the laser frequency is detuned to the original plasmonic cavity frequency ω_c instead of the shifted one ω_c'.

Red-Detuned Laser Illumination: Phonon Saturation. If we illuminate the system with a red-detuned laser ($\hbar\omega_l = \hbar\omega_c' - 236$ meV), the vibrational damping rate is larger than the pumping rate $\Gamma_{ss}^- > \Gamma_{ss}^+$. The optomechanical damping rate is thus positive $\Gamma_s^{opt} > 0$, and the effective phonon decay rate becomes larger $\gamma_s + N\Gamma_s^{opt} > \gamma_s$. For sufficiently strong illumination, the larger loss compensates the linear increase of the vibrational pumping rate with increasing laser intensity in eqs 4 and 5. As a result, the incoherent phonon population and noise correlation saturate toward $n_s^{th} + \Gamma_{ss}^+/(N\Gamma_s^{opt})$ and $\Gamma_{ss}^+/(N\Gamma_s^{opt})$, respectively (Figure 2c), which can be derived by considering the limit of large laser intensity in eqs 4 and 5 (with $\Gamma_{ss}^{st} \propto I_{las}$, $\Gamma_s^{opt} \propto I_{las}$ and $n_s^{th} \ll 1$). Because of the saturation, the Stokes and anti-Stokes signal become again linearly dependent on the laser intensity (Figure 2f and eqs 2 and 3 or eqs 6 and 7).

In a similar manner as for the parametric instability, the saturation becomes significant for $N\Gamma_s^{opt} \approx \gamma_s$, so that a larger number of molecules allow for reaching this effect for weaker (but still very strong) laser intensity. This effect is again due to the coupling with the collective bright mode of the molecules (section S4 in the Supporting Information). Furthermore, the expressions derived above indicate that larger N leads to a $\approx 1/N$ decrease of the saturated value of the noise correlation, as shown by Figure 2c. The incoherent phonon population remains nonetheless larger than n_s^{th}.

The dependence of the noise correlation and the phonon population on N is a signature of collective effects. However, we see that the integrated Stokes intensity per molecule does not depend on N for any laser intensity and the anti-Stokes signal per molecule becomes independent of N for very strong illumination (Figure 2f). These behaviors occur because the superradiant contribution to the SERS signal that scales as N^2 is compensated by the $1/N$ decrease of the incoherent phonon population and the noise correlation, so that the signal becomes proportional to the number of molecules (i.e., constant after normalization by N). In fact, the presence of collective effects for strong I_{las} and red-detuned illumination may be more easily demonstrated by studying the change of the Raman lines, which would become broader and shifted as the laser becomes more intense (see section S5.2 in the Supporting Information).

Last, we note that in typical cavity-optomechanical systems, characterized by low mechanical frequencies and thus large thermal population n_s^{th}, a positive value of Γ_s^{opt} is often exploited to reduce the phonon population below the thermal value, i.e. to cool the sample.[43] In contrast, we have shown (Figure 2c) that in our system, which exhibits a much larger vibrational frequency, the incoherent phonon population remains always larger than n_s^{th}. This difference occurs because the optomechanically induced phonon decay rate of the thermally activated molecules equals $\Gamma_s^{opt} n_s^{th}$ (corresponding to the negative term in the numerator of eqs 4 and 5), which scales with the thermal phonon population. For a large n_s^{th}, as typical in cavity-optomechanics, this decay rate will dominate over the incoherent pumping rate Γ_{ss}^+ and thus the cooling can occur. In contrast, in our system Γ_{ss}^+ remains the larger of the two contributions and thus the system is heated, i.e. $n_s > n_s^{th}$. Thus, when the laser is red-detuned with respect to the plasmon, we refer to the regime of large intensities as the saturation regime, instead of the cooling regime as often referred in cavity optomechanics.

Collective Effects Landscape. We summarize the collective effects in Figure 3, where the integrated anti-Stokes signal is shown as a function of the number of molecules N for blue-detuned laser illumination of different intensities I_{las}. The results for the Stokes signal under a blue-detuned laser illumination, and for the anti-Stokes signal under red- and zero-detuned illumination are shown in section S5.4 of the Supporting Information. Here, we plot the total signal from all the molecules and do not normalize them by N. For small I_{las} (the thermal regime, red dotted line) the total signal scales linearly with N, as it should occur for independent molecules, which indicates the absence of collective effects. For intermediate I_{las} (the vibrational pumping regime, blue dashed line), we find the first collective effect, namely the quadratic scaling of the anti-Stokes SERS signal with N that we have explained as a superradiant phenomenon. Last, for the strongest laser intensity I_{las} (the parametric instability regime, black solid line), the signal increases faster than N^2, which is a manifestation of the second collective effect, namely the influence of N on the effective phonon decay rate and thus on the threshold laser intensity to achieve the parametric instability. This change of the

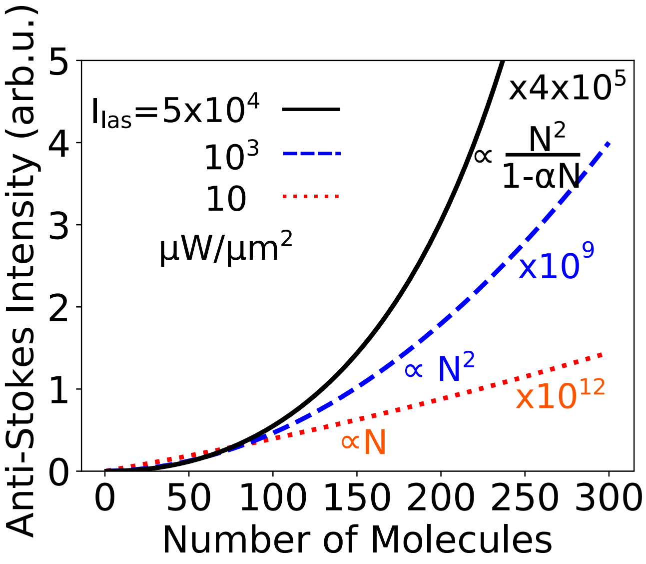

Figure 3. Integrated anti-Stokes intensity as a function of the number of molecules N (from 1 to 300) for molecules in a plasmonic cavity (as in Figure 2) illuminated by a blue-detuned laser ($\hbar(\omega_l - \omega_c') = 236$ meV) of intensity (red dotted line) $I_{las} = 10\ \mu W/\mu m^2$, (blue dashed line) $I_{las} = 10^3\ \mu W/\mu m^2$, and (black solid line) $I_{las} = 5 \times 10^4\ \mu W/\mu m^2$. The signal is scaled as indicated in the figure, and we assume no homogeneous broadening $2\chi_s = 0$, phonon decay rate $\hbar\gamma_s = 0.07$ meV, and temperature $T = 290$ K.

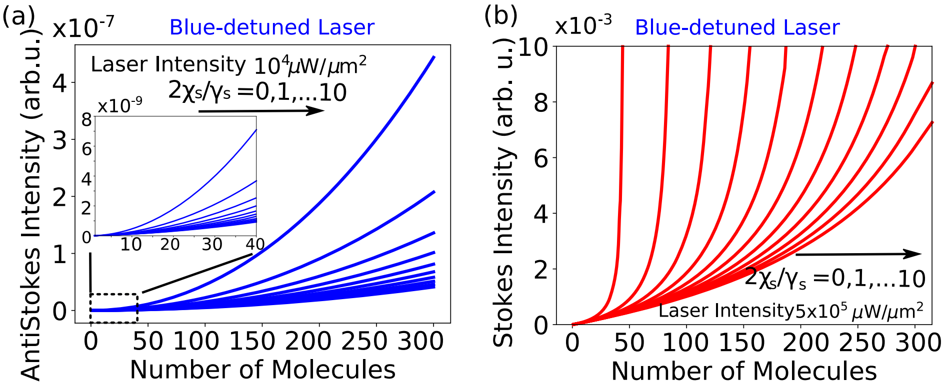

Figure 4. Influence of homogeneous broadening ($2\chi_s = 0, \gamma_s$, to $10\gamma_s$) on the integrated (a) anti-Stokes and (b) Stokes intensity from $N = 1$ to 300 molecules. The system is illuminated by a blue-detuned laser ($\hbar(\omega_l - \omega_c') = 236$ meV) of intensity (a) $I_{las} = 10^4$ μW/μm^2 and (b) $I_{las} = 5 \times 10^5$ μW/μm^2. In all panels,we assume $\hbar\gamma_s = 0.07$ meV and temperature $T = 290$ K. The inset in (a) is a zoom-in to the region of small N.

threshold can be understood as the consequence of coupling with the bright collective mode with a strength $\sqrt{N}g_s$ or the multiple interaction paths of the Raman scattering in Figure 1c,d. More precisely, in this case, the signal scales approximately as $N^2/(1 - \alpha N)$, with $\alpha = |\Gamma_s^{opt}|/\gamma_s$ a constant proportional to I_{las}. Thus, for fixed I_{las}, an increasing number of molecules brings the laser illumination closer to the condition $\alpha N = 1$ to achieve the parametric instability.

CONTRIBUTIONS TO THE RAMAN LINE WIDTH

We have so far focused on a simple system where the molecules are identical and the only loss mechanism experienced by them is the phonon decay. In real experiments, however, the situation can be more complex. For example, the molecules can show small variations of vibrational frequencies (inhomogeneous broadening) and the width of the Raman lines could be affected not only by the phonon decay but also by other phenomena, such as spectral wandering and collision-induced pure dephasing (which leads to homogeneous broadening[54]). To our knowledge, it is still not well understood to what extent the homogeneous and inhomogeneous broadening influence the vibrational dynamics. However, it has been shown that they can affect strongly the collective response of atomic ensembles.[65] Thus, it can be important to examine their impact on the collective effects of SERS.

Influence of Homogeneous Broadening. We model the homogeneous broadening by a Lindblad term in the master equation with a dephasing rate χ_s (see Methods section). Considering again identical molecules and exploiting the permutation symmetry, we obtain

$$c_{ss'} = \frac{\gamma_s}{\gamma_s + 2\chi_s} \frac{\Gamma_{ss}^{+} - \Gamma_s^{opt} n_s^{th}}{\gamma_s + \frac{2\chi_s + N\gamma_s}{\gamma_s + 2\chi_s}\Gamma_s^{opt}} \tag{8}$$

$$n_s = n_s^{th} + \frac{\Gamma_{ss}^{+} - \Gamma_s^{opt} n_s^{th}}{\gamma_s + \frac{2\chi_s + N\gamma_s}{\gamma_s + 2\chi_s}\Gamma_s^{opt}} \tag{9}$$

for the noise correlation and the incoherent phonon population, respectively. Comparing these equations with eqs 4 and 5, we observe a change in the denominator that can be understood as a reduction of the effective number of molecules contributing to the collective response from N to $N_{eff} = (2\chi_s + N\gamma_s)/(\gamma_s + 2\chi_s)$. In addition, the noise correlation is also reduced by $\gamma_s/(\gamma_s + 2\chi_s)$ with respect to the value for $2\chi_s = 0$. The integrated Stokes and anti-Stokes intensity can still be computed with eqs 2 and 3, which do not depend explicitly on χ_s, so that they are affected by the pure dephasing only due to their dependence on the noise correlation and incoherent phonon population. The derivation of all the expressions can be found in sections S1–S3 in the Supporting Information, where a sufficiently small coherent amplitude β_s is assumed.

We illustrate next the effect of the homogeneous broadening $2\chi_s$ on the collective response of systems under blue-detuned laser illumination and for the phonon decay rate $\hbar\gamma_s = 0.07$ meV. Figure 4a demonstrates that, for moderate illumination $I_{las} = 10^4$ μW/μm^2 (the vibrational pumping regime) and all values of $2\chi_s$ considered, the evolution of the integrated anti-Stokes signal as more molecules are present is dominated by the superradiant contribution that scales quadratically with the number of molecules ($\propto N^2$). This quadratic contribution becomes weaker for increasing $2\chi_s$ but remains significant for all values considered, which indicates that the superradiant anti-Stokes scattering is robust to the homogeneous broadening. We can quantify this statement by inserting eqs 8 and 9 into eq 3 to obtain the term scaling with N^2 as approximately $N^2\Gamma_{ss}^{-}\Gamma_{ss}^{+}/(\gamma_s{+}2\chi_s)$, for the moderate intensity considered. In addition, this expression also indicates a quadratic scaling with laser intensity because $\Gamma_{ss}^{-} \propto I_{las}$ and $\Gamma_{ss}^{+} \propto I_{las}$.

Figure 4b shows that the larger the homogeneous broadening $2\chi_s$ the more molecules are required to observe the divergent Stokes signal at strong laser illumination (here $I_{las} = 5 \times 10^5$ $\mu W/\mu m^2$), i.e. the parametric instability. The increase of the number of molecules, however, is moderate and progressive. More precisely, the number of molecules required to reach the divergence is $N = (\gamma_s + 2\chi_s)/|\Gamma_s^{opt}| - 2\chi_s/\gamma_s$ (obtained by setting the denominator in eq 9 as zero). In short, the collective effects are robust to the homogeneous broadening.

Influence of Inhomogeneous Broadening. We consider next the inhomogeneous broadening due to slight variations of the vibrational frequencies in different molecules, which could be caused, for example, by different Stark shifts induced by the local environment or by different chemical interaction with the metal atoms of the plasmonic system.[68] We model the inhomogeneous broadening with a Gaussian distribution $[\sigma\sqrt{2\pi}]^{-1}\exp\{-(\omega_s - \mu)^2/(2\sigma^2)\}$ of the vibrational frequencies ω_s characterized by the mean $\hbar\mu = 196.5$ meV and the standard deviation σ (corresponding to a line width of the distribution $\chi_G = 2\sqrt{2\ln 2}\,\sigma$). An example of the random frequency distribution is shown by the histogram in Figure 5a.

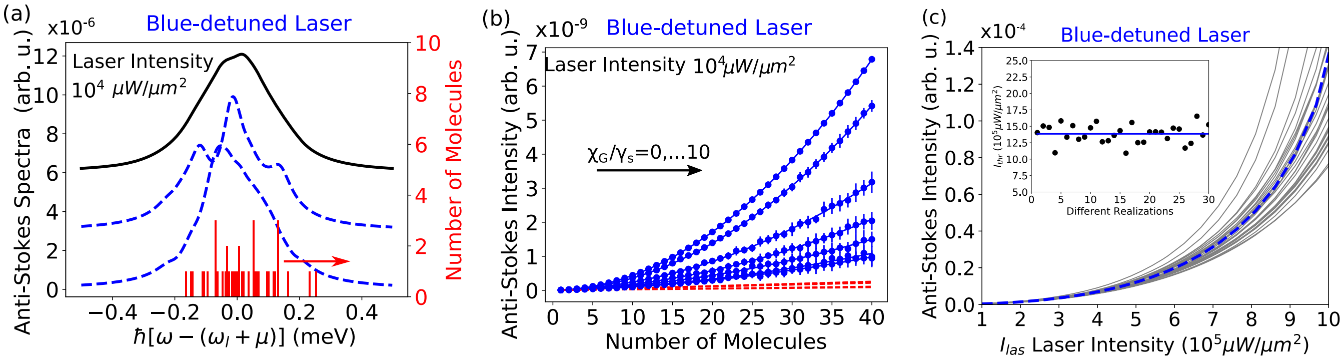

Figure 5. Influence of inhomogeneous broadening χ_G on the anti-Stokes spectra. (a) Two examples of spectra (blue dashed curves, left axis) for 40 molecules and the average over 40 spectra (black solid curve, left axis) as well as one histogram of vibrational frequencies (red bars, right axis). The spectra are shifted vertically for visibility. The x-axis indicates the shift with respect to the mean of the anti-Stokes Raman frequencies $\omega_l + \mu$. (b) Mean (blue dots) and 1-sigma standard deviation (blue bars) of the integrated anti-Stokes intensity versus number of molecules (from $N = 1$ to 40) for increasing χ_G (varying as $0, 1, 3, 5, 7, 9, 10\gamma_s$). The statistics are obtained with 30 realizations. The average is fitted to $\alpha N + \beta N^2$ and the linear term αN is shown with red dashed lines. In (a) and (b) we consider moderate laser intensity $I_{las} = 10^4\ \mu\mathrm{W}/\mu\mathrm{m}^2$. (c) shows the integrated anti-Stokes intensity from 40 molecules and $\hbar\chi_G = 0.21$ meV as a function of I_{las} (close to the parametric instability). The gray solid curves show 30 realizations, and the blue dashed curve shows the average. The inset shows the laser threshold intensity I_{thr} of the parametric instability. In all panels, we consider blue-detuned laser illumination ($\hbar(\omega_l - \omega_c') = 236$ meV), phonon decay rate $\hbar\gamma_s = 0.07$ meV, and temperature $T = 290$ K.

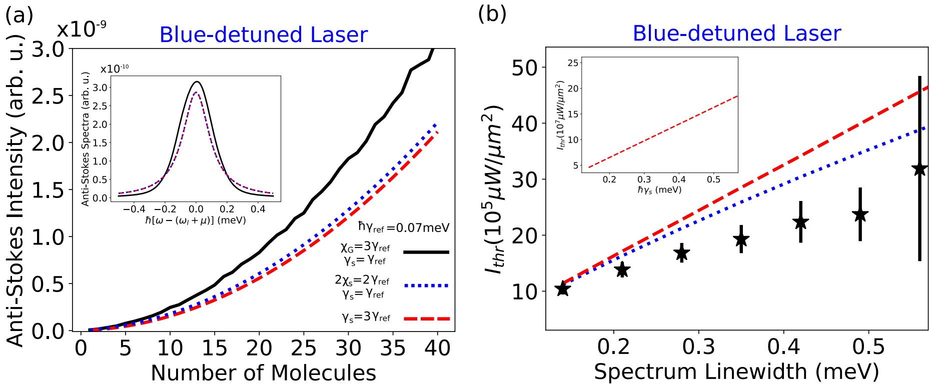

Figure 6. Comparison of the different origins of the Raman line width. (a) Integrated anti-Stokes intensity for increasing number of molecules, illuminated by a blue-detuned laser of intensity $I_{las} = 10^4\ \mu\mathrm{W}/\mu\mathrm{m}^2$ and for phonon decay rate $\hbar\gamma_s = 0.21$ meV and no homogeneous or inhomogeneous broadening (red dashed curves), homogeneous broadening $2\hbar\chi_s = 0.14$ meV and decay rate $\hbar\gamma_s = 0.07$ meV (blue dotted lines), and inhomogeneous broadening $\hbar\chi_G = 0.21$ meV and decay rate $\hbar\gamma_s = 0.07$ meV (black solid line). The inset shows the corresponding anti-Stokes spectra for the three cases for 40 molecules and under weak laser illumination $I_{las} = 10\mu W/\mu m^2$. (b) Laser intensity threshold I_{thr} to achieve the parametric instability for 40 molecules plotted against the line width of the Raman lines γ_T that would be obtained at low laser intensity. The line width for the three situations is estimated as $\gamma_T = \gamma_s$ (only phonon decay, red dashed curves), $\gamma_T = 2\chi_s + \gamma_s$ (including homogeneous broadening, blue dotted lines) and $\gamma_T = \chi_G$ (including inhomogeneous broadening, black stars for the average and vertical bars for the 1-sigma standard deviation). In the latter two cases, γ_s is fixed to 0.07 meV and we modify $2\chi_s$ or χ_G. The inset shows I_{thr} for increasing γ_s in the case of a single molecule. In all panels, we assume $\hbar(\omega_l - \omega_c') =$ 236 meV and temperature $T = 290$ K. The results plotted for $\chi_G > 0$ are computed from 30 different realizations.

We compute the Raman spectra by solving numerically the equations given in section S2 of the Supporting Information for systems with up to 40 molecules. The blue dashed lines in Figure 5a show two examples of the anti-Stokes Raman spectra for $I_{las} = 10^4\ \mu\mathrm{W}/\mu\mathrm{m}^2$, 40 molecules, and $\chi_G = 3\gamma_s$ ($\hbar\gamma_s = 0.07$ meV, spectra shifted vertically for visibility). The average of such anti-Stokes spectra over 30 simulations is shown by the solid line and it shows a smooth single peak similar to those measured in typical experiments. For the parameters considered in Figure 5, the line width of the resulting spectra is approximately χ_G.

We show in Figure 5b the dependence of the integrated anti-Stokes spectra on the number of molecules N for different values of inhomogeneous broadening χ_G (relative to the phonon decay rate $\hbar\gamma_s = 0.07$ meV). The integral is performed numerically over a finite frequency range, which can lead to a small under-estimation of the values (we estimate the error at around 10%). We show the mean and standard deviation of 30 realizations for laser illumination $I_{las} = 10^4\ \mu\mathrm{W}/\mu\mathrm{m}^2$ (the vibrational pumping regime). For a given χ_G the results depend only weakly on the exact random distribution of the vibrational frequencies, as indicated by the small values of the standard deviations. As for the homogeneous broadening, increasing χ_G reduces the mean intensity but does not affect the quadratic scaling of the signal. To be more precise, we fit the mean intensity to $\alpha N + \beta N^2$ (with α, β as fitting parameters) and find that the linear contribution αN (red dashed lines) is negligible. The decrease of the quadratic contribution with increasing χ_G is moderate and it becomes about three times smaller when the ratio χ_G/γ_s increases from zero (i.e., identical vibrational frequencies) to three. The latter χ_G/γ_s ratio is close to the value reported experimentally in ref 68. We thus conclude that the superradiant N^2 scaling can survive in the presence of significant inhomogeneous broadening.

Last, Figure 5c shows the integrated anti-Stokes intensity for $N = 40$ molecules, the inhomogeneous broadening $\chi_G/\gamma_s = 3$, and increasing laser intensity I_{las}. The strongest intensities considered are close to the value leading to the divergent SERS signal (the parametric instability). The gray lines show 30 realizations and the blue solid line their average. The difference between the individual realizations of the results becomes larger as I_{las} increases, but the qualitative behavior remains the same for all realizations. To characterize the variation quantitatively, we fit the results for all realizations with the expression $\propto I_{las}^2/(1 - I_{las}/I_{thr})$, with I_{thr} the threshold intensity at which the signal diverges. We plot the resulting I_{thr} in the inset of Figure 5c. We obtain an average threshold of 1.38×10^6 μW/μm^2 and the thresholds for different realizations differ from this average by a maximum of ±21%. In conclusion, we have seen that the strength of the collective effects is reduced by increasing inhomogeneous broadening but that the change is gradual and moderate.

Equivalence of Homogeneous and Inhomogeneous Contributions to the Collective SERS Signal. In the previous sections we have considered three mechanisms (phonon decay, homogeneous broadening, and inhomogeneous broadening) contributing to the width of the Raman lines. It is however not evident if the collective effects depend on which of these mechanisms are present in a given experiment or whether it is only the value of the line width (at low laser intensity I_{las}) that is important. We investigate this question with a system illuminated by a blue-detuned laser ($\hbar(\omega_l - \omega_c') = 236$ meV). As in the previous subsection, when the inhomogeneous broadening is present we average 30 realizations of molecules with slightly different (random) vibrational frequencies. For consistency, in this subsection we calculate the integrated Raman signal by numerical integration of the Raman spectra.

Figure 6a compares the integrated anti-Stokes intensity in the vibrational pumping regime ($I_{las} = 10^4$ μW/μm^2) as a function of the number of molecules for a situation where the Raman line width is only due to (i) the phonon decay rate $\hbar\gamma_s = 0.21$ meV (red dashed lines) and two other situations where the Raman line width is determined by (ii) a weaker decay rate $\hbar\gamma_s = 0.07$ meV and a homogeneous broadening $2\chi_s = 0.14$ meV (blue dotted line) or (iii) an inhomogeneous broadening $\chi_G = 0.21$ meV (solid black lines). These values are chosen because they lead to similar anti-Stokes spectra in the thermal regime, as demonstrated in the inset for $I_{las} = 10$ μW/μm^2. Notice that the spectra have Lorentzian shape in the first two cases but a Gaussian-like shape in the last one. We observe that the three cases result in a very similar N^2 superradiant scaling. There is some difference in the results for the larger number of molecules, but the difference remains moderate.

Further, we show in Figure 6b the laser threshold intensity I_{thr} to achieve the parametric instability for 40 molecules as a function of the total level of losses for the three situations under consideration. We quantify the losses by the approximate line width γ_T that would be obtained for low laser intensity. For the three different situations under study, γ_T corresponds to (i) $\gamma_T = \gamma_s$ with $2\chi_s = \chi_G = 0$ (red dashed lines), (ii) $\gamma_T = 2\chi_s + \gamma_s$ with $\chi_G = 0$ (blue dotted line) or (iii) $\gamma_T = \chi_G$ with $2\chi_s = 0$ (black stars and black error bars). In the last situation, the effect of the phonon decay γ_s on the broadening is small for $\chi_G \gtrsim \gamma_s$ and thus we have neglected it for the estimation of γ_G. For the first scenario, we vary the phonon decay rate γ_s, while for the other two we fix $\hbar\gamma_s = 0.07$ meV and vary either $2\chi_s$ or χ_G. We obtain I_{thr} from the theoretical expressions when the inhomogeneous broadening is absent, and otherwise from fitting the calculated results, as discussed in the previous subsections.

The situation including inhomogeneous broadening ($\chi_G > 0$) results in the smallest average I_{thr} (black stars) for all γ_T, although the variation from realization to realization increases as the line width becomes larger (black error bars). For the first situation with only phonon decay γ_s (dashed red line), I_{thr} scales linearly with the line width γ_T and for large loses is about two times larger than the situation with inhomogeneous broadening for the same γ_T. Last, the situation including homogeneous broadening ($2\chi_s > 0$) leads to intermediate values of I_{thr} for the largest γ_T considered (dotted blue line), while for $\gamma_T \leqslant 0.21$ meV I_{thr} becomes similar to the results with just the phonon decay. For reference, the inset of Figure 6b gives the laser threshold for a single molecule and no broadening, which is about 40 times larger than those for 40 molecules.

We have thus shown that the mechanisms behind the width of the Raman lines can result in some differences in the SERS signal, but these differences are generally small or moderate. It thus seems possible to predict the general impact of collective effects in the emitted signal even if the exact mechanism inducing the width of the Raman lines is not known. However, the precise mechanism can influence the phonon population (see the difference between increasing γ_s or χ_s in eq 9).

■ SUMMARY AND DISCUSSION

In summary, we have developed a model based on molecular optomechanics to describe surface-enhanced Raman scattering (SERS) from many molecules near a metallic nanostructure. The resulting equations can be solved analytically for identical molecules or numerically for more general systems. We use the basis of individual molecules and verify that the equations can be reduced to those obtained using collective modes for a situation involving identical molecules and no homogeneous broadening.

Our analysis indicates that the collective effects in SERS are mediated by the quantum correlations between molecules, and it reveals the conditions under which the collective response could emerge in experiments. More precisely, we focus on two types of collective effects by analyzing the evolution of the Raman scattering with increasing number of molecules N.

The first collective effect is a $1/N$ dependence of the threshold laser intensity required to observe: (i) the divergence and narrowing of the SERS lines (the parametric instability) for a laser blue-detuned with respect to the plasmonic resonance, and (ii) the saturation of the phonon population and the broadening of the SERS lines under a red-detuned laser. The observation of these phenomena requires very intense illumination (likely a pulsed laser) even for many molecules, vibrational modes with large Raman tensor, and low phonon decay rate. The required intensity could be reduced in systems with a large chemical enhancement of the Raman tensor. However, other mechanisms might affect the response of the system for the large intensities involved, such as the dissociation of the molecules, the presence of vibrational anharmonicities or additional nonlinearities introduced by (strongly detuned) molecular electronic transitions. Thus, the experimental demonstration of these phenomena would likely require very carefully designed systems. In addition, for such strong illumination, a more rigorous treatment of the laser-plasmon coupling beyond the rotating wave-approximation may introduce some corrections to our results.

As the second collective effect, we show that the SERS signal increases quadratically with the number of molecules for red-, blue-, or zero-detuned laser illumination; that is, we establish on a firm theoretical basis the effect of superradiant SERS scattering. The laser intensity to observe this effect in the anti-Stokes scattering at room temperature is about 3 orders of magnitude smaller than the intensity to observe the parametric instability and phonon-population saturation or to observe superradiance in the Stokes scattering. Further, the intensity required to observe the superradiant anti-Stokes scattering can be significantly reduced by working at low temperature. Thus, this collective effect seems particularly attractive for experimental demonstration with continuous or pulsed lasers.

To better understand the main features of collective effects in SERS, we have focused on a situation where molecules that support a single vibration interact with each other via their coupling to a single plasmonic mode, ignoring direct intermolecular interaction.[44] Our results are thus better suited, for example, for well-separated molecules and laser illumination of sufficiently low frequency so that the multiplicity of high-order plasmonic modes (the pseudomode[69]) does not contribute significantly. However, this model can be extended to describe more general situations that might involve direct intermolecular interactions, multiple Raman-active vibrations, multiple plasmonic modes, or infrared active vibrations. Further, we initially considered a relatively simple situation of identical molecules with no decay channel beyond standard phonon decay, but we also demonstrated that the collective response survives in more complex scenarios. Specifically, we verify that the collective phenomena are affected only moderately by the presence of homogeneous and inhomogeneous broadening of the molecular vibrations, so that the effects reported here seem robust.

In conclusion, our results establish a general theoretical framework to study collective effects in SERS and suggest that novel collective phenomena can be accessible to experiments under realistic laser illumination.

■ METHODS

We apply open quantum system theory[60] to describe SERS, including all relevant incoherent processes. In this description, the dynamics are governed by the quantum master equation for the density operator ρ:

$$\partial_t\rho = -\frac{i}{\hbar}[H, \rho] + \mathcal{D}[\rho] \tag{10}$$

with the full Hamiltonian $H = H_{vib} + H_{cav} + H_{las} + H_{int}$ and the following Lindblad terms

$$\begin{aligned}\mathcal{D}[\rho] &= (\kappa/2)\mathcal{D}[a]\rho + \sum_s \chi_s \mathcal{D}[b_s^\dagger b_s]\rho \\ &+ \sum_s (\gamma_s/2)\{(n_s^{th} + 1)\mathcal{D}[b_s]\rho + n_s^{th}\mathcal{D}[b_s^\dagger]\rho\}\end{aligned} \tag{11}$$

where we introduce the superoperator (for any operator o) $\mathcal{D}[o]\rho = 2o\rho o^\dagger - (o^\dagger o\rho + \rho o^\dagger o)$ and the thermal phonon population $n_s^{th} = [e^{\hbar\omega_s/k_B T} - 1]^{-1}$ at temperature T (k_B is the Boltzmann constant). The first Lindblad term describes the damping of the plasmonic mode at rate κ, the second the homogeneous broadening due to the pure dephasing rate χ_s, and the last two the phonon decay at rate γ_s and the thermal pumping of the molecular vibrations, respectively.

To solve the master equation (eq 9), we first go to a frame rotating with the laser frequency and then linearize the optomechanical interaction H_{int} and finally eliminate the plasmonic degree of freedom. In the end, we obtain the following effective master equation for the reduced density operator ρ_v of the vibrational noise operator $\delta b_s = b_s - \beta_s$ (with coherent amplitudes $\beta_s = \mathrm{tr}\{b_s\rho\}$):

$$\partial_t\rho_v = -\frac{i}{\hbar}[H_v, \rho_v] + \mathcal{D}_v[\rho_v] \tag{12}$$

with Hamiltonian

$$H_v = \sum_s \hbar\omega_s \delta b_s^\dagger \delta b_s - \sum_{s,s'} (\hbar/2)(\Omega_{ss'}^+ + \Omega_{s's}^-)\delta b_s^\dagger \delta b_{s'} \tag{13}$$

and Lindblad terms

$$\begin{aligned}\mathcal{D}_v[\rho_v] &= \sum_s \chi_s \mathcal{D}[\delta b_s^\dagger \delta b_s]\rho_v \\ &+ \sum_s (\gamma_s/2)((n_s^{th} + 1)\mathcal{D}[\delta b_s]\rho_v + n_s^{th}\mathcal{D}[\delta b_s^\dagger]\rho_v) \\ &+ (1/2)\sum_{s,s'} (\Gamma_{ss'}^- \mathcal{D}[\delta b_s , \delta b_{s'}^\dagger]\rho_v + \Gamma_{ss'}^+ \mathcal{D}[\delta b_s^\dagger, \delta b_{s'}]\rho_v)\end{aligned} \tag{14}$$

for superoperator $\mathcal{D}[o, p]\rho = 2o\rho p - (po\rho + \rho po)$ (for any pair of operators o, p). The coherent amplitude of the vibration $\beta_s = g_s|\alpha|^2/(\omega_s - i(\gamma_s/2 + \chi_s))$ can be computed from the coherent amplitude of the plasmon $\alpha = \Omega/(i(\omega'_c - \omega_l) + \kappa/2)$. The value of $|\beta_s|^2$ is shown in section S5.1 in the Supporting Information, and it is much smaller than the incoherent phonon population $n_s \equiv \langle \delta b_s^\dagger \delta b_s \rangle$ except for extremely large laser intensity.

The derivation of these expressions and the values of the different parameters are given in section S1 of the Supporting Information. Briefly, the parameters $\Omega_{ss'}^+$, $\Omega_{ss'}^-$ can be obtained from the imaginary part of the spectral density $S_{ss'}(\omega)$ at the Stokes $\omega = \omega_l - \omega_s$ and anti-Stokes lines $\omega = \omega_l + \omega_s$, respectively, and describe the plasmon-induced frequency shift ($s = s'$) and the plasmon-mediated coherent coupling ($s \neq s'$). Similarly, the parameters $\Gamma_{ss'}^+$,$\Gamma_{ss'}^-$ can be calculated from the real part of $S_{ss'}(\omega)$ and describe the plasmon-induced pumping Γ_{ss}^+ and damping Γ_{ss}^- and the plasmon-mediated dissipative coupling ($\Gamma_{ss'}^+$ and $\Gamma_{ss'}^-$ with $s \neq s'$). $S_{ss'}(\omega)$ depends on the optomechanical couplings $g_s g_{s'}$ of two molecules, the frequency detuning between the laser and the plasmonic cavity mode, the plasmonic losses, and the laser intensity. In section S1.3 of the Supporting Information, we show the dependence of $\Omega_{ss}^\pm$ and $\Gamma_{ss}^\pm$ on laser frequency, which is key to understand the collective effects under intense laser illumination.

From eq 12 we can derive the equations $\partial_t\langle o \rangle = \mathrm{tr}\{o\partial_t\rho_v\} = \frac{i}{\hbar}\langle [H_v, o]\rangle + \mathrm{tr}\{o\mathcal{D}_v[\rho_v]\}$ for the expectation values of different operators ($\langle o \rangle = \mathrm{tr}\{o\rho_v\}$, with *tr* the trace). In particular, we derive a closed set of equations for the incoherent phonon number $\langle \delta b_s^\dagger \delta b_s \rangle = n_s$ and the noise correlations $\langle \delta b_s^\dagger \delta b_{s'} \rangle = c_{ss'}$ ($s \neq s'$). These equations can be solved for systems with a significant number of molecules.

Last, we obtain the Stokes and anti-Stokes SERS signal from the correlations of the noise dynamics according to[55] $S^{st,as}(\omega) \propto \omega^4 \sum_{ss'} \Gamma_{ss'}^{+,-} \mathrm{Re} S_{ss'}^{st,as}(\omega - \omega_l)$ with $S_{ss'}^{st}(\omega) = \int_0^\infty d\tau e^{-i\omega\tau}\langle \delta b_s(\tau)\delta b_{s'}^\dagger(0)\rangle$ and $S_{ss'}^{as}(\omega) = \int_0^\infty d\tau e^{-i\omega\tau}\langle \delta b_s^\dagger(\tau)\delta b_{s'}(0)\rangle$, respectively. According to the quantum regression theorem,[61] the two-time correlations $\langle \delta b_s(\tau)\delta b_{s'}^\dagger(0)\rangle$ and $\langle \delta b_s^\dagger(\tau)\delta b_{s'}(0)\rangle$ follow the same equations as $\langle \delta b_s \rangle$ and $\langle \delta b_s^\dagger \rangle$, but with initial conditions $\langle \delta b_s \delta b_{s'}^\dagger \rangle_{ste}$ and

$\langle \delta b_s^\dagger \delta b_{s'} \rangle_{ste}$. Here, the label "*ste*" refers to the steady-state and the equations for $\langle \delta b_s \rangle$ and $\langle \delta b_s^\dagger \rangle$ are obtained from $\partial_t \langle o \rangle = \mathrm{tr}\{ o \partial_t \rho_v \}$.

■ ASSOCIATED CONTENT

Supporting Information

The Supporting Information is available free of charge at https://pubs.acs.org/doi/10.1021/acsphotonics.0c00032.

> Derivation of effective master equation, equations for incoherent phonon population and noise correlation, expression for SERS spectrum, analytic expressions for systems with identical molecules, collective oscillator model and other supplemental results (coherent phonon population, shift, narrowing and broadening of the SERS lines, laser threshold for molecules with different Raman tensor, collective effects landscape under blue-, zero-, and red-detuned laser illumination, and influence of phonon-induced plasmon shift) (PDF)

■ AUTHOR INFORMATION

Corresponding Authors

Yuan Zhang − *Donostia International Physics Center, 20018 Donostia-San Sebastián, Spain; School of Physics and Microelectronics, Zhengzhou University, 450052 Zhengzhou, China*; Email: yzhuaudipc@zzu.edu.cn

Javier Aizpurua − *Donostia International Physics Center, 20018 Donostia-San Sebastián, Spain; Center for Material Physics (CSIC - UPV/EHU), 20018 Donostia-San Sebastián, Spain*; orcid.org/0000-0002-1444-7589; Email: aizpurua@ehu.eus

Ruben Esteban − *Donostia International Physics Center, 20018 Donostia-San Sebastián, Spain; IKERBASQUE, Basque Foundation for Science, 48013 Bilbao, Spain*; orcid.org/0000-0002-9175-2878; Email: ruben_esteban@ehu.eus

Complete contact information is available at:
https://pubs.acs.org/10.1021/acsphotonics.0c00032

Notes

The authors declare no competing financial interest.
The data used for the figures presented in this paper can be found in https://digital.csic.es/handle/10261/212742.

■ ACKNOWLEDGMENTS

We would like to thank Mikolaj K. Schmidt, Roberto A. Boto, and Jeremy J. Baumberg for fruitful discussions. We acknowledge the project FIS2016-80174-P from the Spanish Ministry of Science, Innovation and Universities, the project PI2017-30 of the Departamento de Educación, Política Lingüística y Cultura of the Basque Government, the project KK-2019/00101 from Eusko Jaurlaritza, the project H-2020-FET, the project H2020-FET Open "THOR" Nr. 829067 from the European Commission, and grant IT1164-19 for consolidated groups of the Basque University, through the Department of Universities of the Basque Government, and the NSFC-DPG joint project Nr. 21961132023.

■ REFERENCES

(1) Moskovits, M. Surface-enhanced Spectroscopy. *Rev. Mod. Phys.* **1985**, *57*, 783.

(2) Ru, E. C. L.; Etchegoin, P. G. *Principles of Surface Enhanced Raman Spectroscopy and Related Plasmonic Effects*; Elsevier: Amsterdam, 2009.

(3) Bharadwaj, P.; Deutsch, B.; Novotny, L. Optical Antennas. *Adv. Opt. Photonics* **2009**, *1*, 438−483.

(4) Mühlschlegel, P.; Eisler, H.-J.; Martin, O. J. F.; Hecht, B.; Pohl, D. W. Resonant Optical Antennas. *Science* **2005**, *308*, 1607−1609.

(5) Sivapalan, S. T.; DeVetter, B. M.; Yang, T. K.; et al. Off-Resonance Surface-Enhanced Raman Spectroscopy from Gold Nano-rod Suspensions as a Function of Aspect Ratio: Not What We Thought. *ACS Nano* **2013**, *7*, 2099−2105.

(6) Taminiau, T. H.; Stefani, F. D.; van Hulst, N. F. Single Emitters Coupled to Plasmonic Nano-antennas: Angular Emission and Collection Efficiency. *New J. Phys.* **2008**, *10*, 105005.

(7) Muskens, O. L.; Giannini, V.; Sánchez-Gil, J. A.; Gómez Rivas, J. Strong Enhancement of the Radiative Decay Rate of Emitters by Single Plasmonic Nanoantennas. *Nano Lett.* **2007**, *7*, 2871−2875.

(8) Rogobete, L.; Kaminski, F.; Agio, M.; Sandoghdar, V. Design of Plasmonic Nanoantennae for Enhancing Spontaneous Emission. *Opt. Lett.* **2007**, *32*, 1623−1625.

(9) Niu, W.; Chua, Y. A. A.; Zhang, W.; Huang, H.; Lu, X. Highly Symmetric Gold Nanostars: Crystallographic Control and Surface-Enhanced Raman Scattering Property. *J. Am. Chem. Soc.* **2015**, *137*, 10460−10463.

(10) Hao, F.; Nehl, C. L.; Hafner, J. H.; Nordlander, P. Plasmon Resonances of a Gold Nanostar. *Nano Lett.* **2007**, *7*, 729−732.

(11) Kumar, P. S.; Pastoriza-Santos, I.; Rodríguez-González, B.; et al. High-yield Synthesis and Optical Response of Gold Nanostars. *Nanotechnology* **2008**, *19*, 015606.

(12) Zhu, W.; Crozier, K. B. Quantum Mechanical Limit to Plasmonic Enhancement as Observed by Surface-Enhanced Raman Scattering. *Nat. Commun.* **2014**, *5*, 5228.

(13) Aizpurua, J.; Bryant, G. W.; Richter, L. J.; García de Abajo, F. J. Optical Properties of Coupled Metallic Nanorods for Field-enhanced Spectroscopy. *Phys. Rev. B: Condens. Matter Mater. Phys.* **2005**, *71*, 235420.

(14) Romero, I.; Aizpurua, J.; Bryant, G. W.; García de Abajo, F. J. Plasmons in Nearly Touching Metallic Nanoparticles: Singular Response in the Limit of Touching Dimers. *Opt. Express* **2006**, *14*, 9988−9999.

(15) Esteban, R.; Borisov, A. G.; Nordlander, P.; Aizpurua, J. Bridging Quantum and Classical Plasmonics with a Quantum-corrected Model. *Nat. Commun.* **2012**, *3*, 825.

(16) Nordlander, P.; Oubre, C.; Prodan, E.; Li, K.; Stockman, M. I.; et al. Plasmon Hybridization in Nanoparticle Dimers. *Nano Lett.* **2004**, *4*, 899−903.

(17) Lombardi, A.; Demetriadou, A.; Weller, L.; Andrae, P.; Benz, F.; Chikkaraddy, R.; Aizpurua, J.; Baumberg, J. J. Anomalous Spectral Shift of Near- and Far-Field Plasmonic Resonances in Nanogaps. *ACS Photonics* **2016**, *3*, 471−477.

(18) Baumberg, J. J.; Aizpurua, J.; Mikkelsen, M. H.; Smith, D. R. Extreme Nanophotonics from Ultrathin Metallic Gaps. *Nat. Mater.* **2019**, *18*, 668−678.

(19) Zhang, R.; Zhang, Y.; Dong, Z.; et al. Chemical Mapping of a Single Molecule by Plasmon-Enhanced Raman Scattering. *Nature* **2013**, *498*, 82−86.

(20) Liu, S.; Müller, M.; Sun, Y.; et al. Resolving the Correlation between Tip-enhanced Resonance Raman Scattering and Local Electronic States with 1 nm Resolution. *Nano Lett.* **2019**, *19*, 5725−5731.

(21) Qiu, X. H.; Nazin, G. V.; Ho, W. Vibrationally Resolved Fluorescence Excited with Submolecular Precision. *Science* **2003**, *299*, 542−54.

(22) Imada, H.; Miwa, K.; Imai-Imada, M.; et al. Real-space Investigation of Energy Transfer in Heterogeneous Molecular Dimers. *Nature* **2016**, *538*, 364−367.

(23) Pettinger, B.; Schambach, P.; J. Villagómez, C.; Scott, N. Tip-enhanced Raman Spectroscopy: Near-fields Acting on a Few Molecules. *Annu. Rev. Phys. Chem.* **2012**, *63*, 379−399.

(24) Stöckle, R. M.; Suh, Y. D.; Deckert, V.; Zenobi, R. Nanoscale Chemical Analysis by Tip-enhanced Raman Spectroscopy. *Chem. Phys. Lett.* **2000**, *318*, 131−136.

(25) Kazuma, E.; Jung, J.; Ueba, H.; Trenary, M.; Kim, Y. Real-space and Real-time Observation of a Plasmon-induced Chemical Reaction of a Single Molecule. *Science* **2018**, *360*, 521−526.

(26) Doppagne, B.; Chong, M. C.; Bulou, H.; et al. Electrofluorochromism at the Single-molecule Level. *Science* **2018**, *361*, 251−255.

(27) Lombardi, J. R.; Birke, R. L.; Lu, T.; Xu, J. Charge-transfer Theory of Surface Enhanced Raman Spectroscopy: Herzberg-Teller Contributions. *J. Chem. Phys.* **1986**, *84*, 4174.

(28) Willets, K. A.; Van Duyne, R. P. Localized Surface Plasmon Resonance Spectroscopy and Sensing. *Annu. Rev. Phys. Chem.* **2007**, *58*, 267−297.

(29) Lin, K.-Q.; Yi, J.; Zhong, J.-H.; et al. Plasmonic Photoluminescence for Recovering Native Chemical Information from Surface-enhanced Raman Scattering. *Nat. Commun.* **2017**, *8*, 14891.

(30) Qin, L.; Zou, S.; Xue, C.; Atkinson, A.; Schatz, G. C.; Mirkin, C. A. Designing, Fabricating, and Imaging Raman Hot Spots. *Proc. Natl. Acad. Sci. U. S. A.* **2006**, *103*, 13300−13303.

(31) Lal, S.; Grady, N. K.; Kundu, J.; et al. Tailoring Plasmonic Substrates for Surface Enhanced Spectroscopies. *Chem. Soc. Rev.* **2008**, *37*, 898−911.

(32) Nie, S. M.; Emory, S. R. Probing Single Molecules and Single Nanoparticles by Surface Enhanced Raman Scattering. *Science* **1997**, *275*, 1102−1106.

(33) Le Ru, E. C.; Etchegoin, P. G. Single-molecule Surface-enhanced Raman Spectroscopy. *Annu. Rev. Phys. Chem.* **2012**, *63*, 65−87.

(34) Kneipp, K.; Wang, Y.; Kneipp, H.; Perelman, L. T.; Itzkan, I.; Dasari, R. R.; Feld, M. S. Single Molecule Detection Using Surface-Enhanced Raman Scattering (SERS). *Phys. Rev. Lett.* **1997**, *78*, 1667−1670.

(35) Cialla-May, D.; Zheng, X.-S.; Weber, K.; Popp, J. Recent Progress in Surface-enhanced Raman Spectroscopy for Biological and Biomedical Applications: from Cells to Clinics. *Chem. Soc. Rev.* **2017**, *46*, 3945.

(36) Kneipp, K.; Wang, Y.; Kneipp, H.; Itzkan, I.; Dasari, R. R.; Feld, M. S. Population Pumping of Excited Vibrational States by Spontaneous Surface-Enhanced Raman Scattering. *Phys. Rev. Lett.* **1996**, *76*, 2444.

(37) Maher, R.; Etchegoin, P.; Le Ru, E.; Cohen, L. A Conclusive Demonstration of Vibrational Pumping Under Surface Enhanced Raman Scattering Conditions. *J. Phys. Chem. B* **2006**, *110*, 11757.

(38) Le Ru, E.; Etchegoin, P. G. Vibrational Pumping and Heating under SERS Conditions: Fact or Myth? *Faraday Discuss.* **2006**, *132*, 63.

(39) Roelli, P.; Galland, C.; Piro, N.; Kippenberg, T. J. Molecular Cavity Optomechanics: a Theory of Plasmon-Enhanced Raman Scattering. *Nat. Nanotechnol.* **2016**, *11*, 164−169.

(40) Schmidt, M. K.; Esteban, R.; Gonzalez-Tudela, A.; Giedke, G.; Aizpurua, J. Quantum Mechanical Description of Raman Scattering from Molecules in Plasmonic Cavities. *ACS Nano* **2016**, *10*, 6291−6298.

(41) Schmidt, M. K.; Esteban, R.; Benz, F.; Baumberg, J. J.; Aizpurua, J. Linking Classical and Molecular Optomechanics Descriptions of SERS. *Faraday Discuss.* **2017**, *205*, 31−65.

(42) Dezfouli, M. K.; Gordon, R.; Hughes, S. Molecular Optomechanics in the Anharmonic Cavity-QED Regime Using Hybrid Metal-Dielectric Cavity Modes. *ACS Photonics* **2019**, *6*, 1400−1408.

(43) Aspelmeyer, M.; Kippenberg, T. J.; Marquardt, F. Cavity Optomechanics. *Rev. Mod. Phys.* **2014**, *86*, 1391.

(44) Ashrafi, S. M.; Malekfar, R.; Bahrampour, A. R.; Feist, J. Optomechanical Heat Transfer between Molecules in a Nanoplasmonic Cavity. *Phys. Rev. A: At., Mol., Opt. Phys.* **2019**, *100*, 013826.

(45) Benz, F.; Schmidt, M. K.; Dreismann, A.; Chikkaraddy, R.; Zhang, Y.; Demetriadou, A.; Carnegie, C.; Ohadi, H.; de Nijs, B.; Esteban, R.; Aizpurua, J.; Baumberg, J. J. Single-molecule Optomechanics in "picocavities. *Science* **2016**, *354*, 726−729.

(46) Roelli, P.; Martin-Cano, D.; Kippenberg, T. J.; Galland, C. Molecular Platform for Frequency Upconversion at the Single-photon Level, arXiv:1910.11395v1.

(47) Lombardi, A.; Schmidt, M. K.; Weller, L.; Deacon, W. M.; Benz, F.; de Nijs, B.; Aizpurua, J.; Baumberg, J. J. Pulsed Molecular Optomechanics in Plasmonic Nanocavities: From Nonlinear Vibrational Instabilities to Bond-Breaking. *Phys. Rev. X* **2018**, *8*, 011016.

(48) Vrijsen, G.; Hosten, O.; Lee, J.; Bernon, S.; Kasevich, M. A. Raman Lasing with a Cold Atom Gain Medium in a High-Finesse Optical Cavity. *Phys. Rev. Lett.* **2011**, *107*, 063904.

(49) Sørensen, A. S.; Mølmer, K. Entangling Atoms in Bad Cavities. *Phys. Rev. A: At., Mol., Opt. Phys.* **2002**, *66*, 022314.

(50) Klinder, J.; Keßler, H.; Wolke, M.; Mathey, L.; Hemmerich, A. Dynamical Phase Transition in the Open Dicke Model. *Proc. Natl. Acad. Sci. U. S. A.* **2015**, *112*, 3290−3295.

(51) Bohnet, J. G.; Chen, Z.; Weiner, J. M.; Meiser, D.; Holland, M. J.; Thompson, J. K. A Steady-state Superradiant Laser with less than One Intracavity Photon. *Nature* **2012**, *484*, 78−81.

(52) Neuman, T.; Esteban, R.; Giedke, G.; Schmidt, M. K.; Aizpurua, J. Quantum Description of Surface-enhanced Resonant Raman Scattering within a Hybrid-optomechanical Model. *Phys. Rev. A: At., Mol., Opt. Phys.* **2019**, *100*, 043422.

(53) Neuman, T.; Aizpurua, J.; Esteban, R. Quantum Theory of Surface-enhanced Resonant Raman Scattering (SERRS) of Molecules in Strongly Coupled Plasmon-exciton Systems. *Nanophotonics* **2020**, *9*, 295−308.

(54) Zhao, Y.; Chen, G. H. Quantum Dissipative Master Equations: Some Exact Results. *J. Chem. Phys.* **2001**, *114*, 10623.

(55) Dezfouli, M. K.; Hughes, S. Quantum Optics Model of Surface-Enhanced Raman Spectroscopy for Arbitrarily Shaped Plasmonic Resonators. *ACS Photonics* **2017**, *4*, 1245−1256.

(56) Esteban, R.; Aizpurua, J.; Bryant, G. W. Strong Coupling of Single Emitters Interacting with Phononic Infrared Antennae. *New J. Phys.* **2014**, *16*, 013052.

(57) Chikkaraddy, R.; de Nijs, B.; Benz, F.; Barrow, S. J.; Scherman, O. A.; Rosta, E.; Demetriadou, A.; Fox, P.; Hess, O.; Baumberg, J. J. Single-molecule Strong Coupling at Room Temperature in Plasmonic Nanocavities. *Nature* **2016**, *535*, 127−130.

(58) Urbieta, M.; Barbry, B.; Zhang, Y.; Koval, P.; Sánchez-Portal, D.; Zabala, N.; Aizpurua, J. Atomic-Scaling Lightning Rod Effect in Plasmonic Picocavities: A Classical View to a Quantum Effect. *ACS Nano* **2018**, *12*, 585−596.

(59) Franke, S.; Hughes, S.; Dezfouli, M. K.; Kristensen, P. T.; Busch, K.; Knorr, A.; Richter, M. Quantization of Quasinormal Modes for Open Cavities and Plasmonic Cavity-QED. *Phys. Rev. Lett.* **2019**, *122*, 213901.

(60) Breuer, H. P.; Petruccione, F. *The Theory of Open Quantum Systems*; Oxford University Press, 2002.

(61) Meystre, P.; Sargent, M. *Elements of Quantum Optics*; Springer-Verlag Berlin and Heidelberg Gmbh & Co. kg, 2010.

(62) Scully, M. O.; Svidzinsky, A. A. The Lamb Shift-Yesterday, Today and Tomorrow. *Science* **2010**, *328*, 1239−1241.

(63) Zhang, Y.; Meng, Q.-S.; Zhang, L.; et al. Sub-nanometre Control of the Coherent Interaction between a Single Molecule and a Plasmonic Nanocavity. *Nat. Commun.* **2017**, *8*, 15225.

(64) Kipf, T.; Agarwal, G. S. Superradiance and Collective Gain in Multimode Optomechanics. *Phys. Rev. A: At., Mol., Opt. Phys.* **2014**, *90*, 053808.

(65) Andreev, A. V.; Emel'yanov, V. I.; Il'inskiĭ, Y. A. Collective Spontaneous Emission (Dicke Superradiance). *Sov. Phys. Usp.* **1980**, *23*, 493−514.

(66) Pustovit, V. N.; Shahbazyan, T. V. Cooperative Emission of Light by an Ensemble of Dipoles Near a Metal Nanoparticle: The Plasmonic Dicke Effect. *Phys. Rev. Lett.* **2009**, *102*, 077401.

(67) Scully, M. O. Collective Lamb Shift in Single Photon Dicke Superradiance. *Phys. Rev. Lett.* **2009**, *102*, 143601.

(68) Etchegoin, P. G.; Ru, E. C. L. Resolving Single Molecules in Surface-Enhanced Raman Scattering within the Inhomogeneous Broadening of Raman Peaks. *Anal. Chem.* **2010**, *82*, 2888−2892.

(69) Delga, A.; Feist, J.; Bravo-Abad, J.; Garcia-Vidal, F. J. Quantum Emitters Near a Metal Nanoparticle: Strong Coupling and Quenching. *Phys. Rev. Lett.* **2014**, *112*, 253601.